Available online at www.sciencedirect.com
ScienceDirect
International Journal of Thermal Sciences 48 (2009) 913–921
International Journal of Thermal Sciences
www.elsevier.com/locate/ijts

Magnetohydrodynamic convection flow from a sphere to a non-Darcian porous medium with heat generation or absorption effects: network simulation

O. Anwar Bég [a], Joaquín Zueco [b,*], R. Bhargava [c], H.S. Takhar [d]

[a] *Engovation Engineering Science Research, 15 Southmere Avenue, Great Horton, Bradford, BD7 3NU, England, UK*
[b] *Departamento de Ingeniería Térmica y Fluidos, Universidad Politécnica de Cartagena, 30203 Cartagena (Murcia), Spain*
[c] *Mathematics Department, Indian Institute of Technology, Roorkee-247667, India*
[d] *Engineering Department, Manchester Metropolitan University, Oxford Rd., Manchester, M1 5GD, UK*

Received 14 November 2007; received in revised form 8 July 2008; accepted 8 July 2008

Available online 3 August 2008

Abstract

The magnetohydrodynamic free convection from a sphere embedded in an electrically-conducting fluid-saturated porous regime with heat generation is examined theoretically and numerically in this paper. A viscous flow model is presented using boundary-layer theory comprising the momentum and heat conservation equations. These coupled non-linear partial differential equations are transformed using appropriate variables to render the problem dimensionless. In the limit of infinite permeability (i.e. infinite Darcy number), the model is shown to reduce to that considered in an earlier study by Molla et al. (2005). Numerical solutions for the non-similar equations are obtained using the Network Simulation Method (NSM). Computations are compared with the earlier studies by Huang and Chen (1987), Molla et al. (2005) and Nazar et al. (2007) and found to be in excellent agreement. Specifically we investigate here in detail the influence of Darcy number (Da), Forchheimer number (Fs), hydromagnetic number (Nm), heat generation parameter (Q) and Grashof number (Gr) on the temperature and velocity fields and derivative functions. An increase in Darcy number accelerates the flow (i.e. increases velocity) but reduces temperature in the fluid. Increasing magnetic field (Nm) causes a reduction in velocity but enhances temperature. With heat generation ($H > 0$), i.e. a heat source, velocity and temperature are increased with the converse behaviour computed for heat absorption, i.e. heat sink ($H < 0$). An increase in inertial porous drag parameter, Fs, causes a decrease in velocity and also surface shear stress. Increasing free convection parameter, Gr, decreases velocity and also surface temperature gradient. The present model finds applications in energy systems and magnetic materials processing.

Keywords: Hydromagnetics; Thermal convection; Buoyancy; Sphere; Darcy number; Forchheimer number; Heat sinks and sources; Energy systems; Network numerical solution

Contents

* Corresponding author.
E-mail addresses: docoanwarbeg@hotmail.co.uk (O.A. Bég), joaquin.zueco@upct.es (J. Zueco), rbharfma@iitr.ernet.in (R. Bhargava), harmindar.takhar@sky.com (H.S. Takhar).

1290-0729/$ – see front matter
doi:10.1016/j.ijthermalsci.2008.07.002

1. Introduction

Heat transfer in electrically-conducting fluids in the presence of magnetic fields has been an area of strong research for many decades. Historically interest sprang in this area following developments in high-speed aerodynamics involving the flight of aircraft in magnetospheric zones where the air becomes electrically-conducting [1]. Early studies considered simple geometric configurations such as flat plates which were used as an approximation for thin airfoils. A seminal study was presented by Rossow [2] who considered the magnetohydrodynamic (MHD) heat transfer problem for the case of an insulated plate, showing that neither flow separation nor reverse flow were produced by a transverse magnetic field. Applications also arise in the sidewalls of large volume MHD energy generators and accelerator devices. Singer [3] reported on the forced and free convection magneto-heat transfer in a vertical channel, showing that magnetic field strongly counters free convection. Keiffer [4] considered the effects of variable electrical conductivity in Hartmann flow and heat transfer in a channel, motivated by the presence of large temperature gradients. Many studies have appeared subsequently examining a wide range of geometries including wedges, ellipses, cones, and spheres. More recent studies have used numerical finite difference techniques to solve the two-dimensional flow problem. For example, recently Bég et al. [5] studied the combined influence of buoyancy and impulsive motion on magneto-convection from a rotating sphere using the Blottner finite difference method, showing that dimensionless surface heat transfer increases with a rise in magnetic field parameter. Heat generation effects on MHD convection from a stationary sphere were reported by Molla et al. [6] using the Keller box difference method who showed that a rise in heat generation boosts the local skin friction coefficient but depresses the local rate of heat transfer. Magnetic field was also shown to reduce velocities but enhance temperatures. Kumari et al. [7] studied numerically the hydromagnetic compressible stagnation point flow from a sphere. Molla et al. [8] presented boundary-layer solutions for magnetohydrodynamic free convection from a sphere with heat generation effects. Alam et al. [9] studied viscous heating effects on hydromagnetic free convection from a sphere. Chamkha and Al-Mudhaf [10] discussed the effect of thermal radiation flux on combined heat and mass transfer in magnetohydrodynamic convection with surface transpiration. Unsteady hydromagnetic convection from a sphere has been extensively analyzed by Takhar and Nath [11] for stagnation-point flow and for a simultaneously translating sphere with free convection effects by Takhar et al [12], respectively. These studies however were confined to *purely fluid* regimes. Porous media however arise frequently in numerous geophysical and also industrial processes. For low velocity scenarios, the *Darcy model* is generally used. At higher velocities in high-porosity regimes, the *Darcy–Forchheimer drag force model* is required. Magnetohydrodynamic convection from spheres and other bodies embedded in porous media has immediate applications in magnetic materials processing and energy systems. Several excellent articles have been communicated discussing hydromagnetic convection in electrically-conducting fluid-saturated porous media. Yih [13] presented numerical finite difference solutions for the influence of viscous dissipation, Joule heating and heat source/sink on non-Darcy MHD natural convection flow over an isoflux permeable sphere in a porous medium for air. Damseh [14] studied magnetohydrodynamic mixed convection flow from a vertical surface embedded in a porous media with thermal radiation effects for both *buoyancy-aiding* and *buoyancy-opposing* flow. Al-Zubi and Duwairi [15] studied hydromagnetic convection boundary layer flow over an ellipse in a Darcian porous regime. Afify [16] numerical analyzed the viscosity and thermal dispersion effects on magnetohydrodynamic natural convection heat and mass transfer from a vertical isothermal surface to saturated non-Darcian porous media with Soret and Dufour effects. Thermophoretic and thermal radiation effects on hydromagnetic free convection in a porous medium were studied by Rashad [17]. El-Kabeir et al. [18] used the Lie group method to study unsteady, three-dimensional laminar hydromagnetic heat transfer from an inclined permeable plate with heat generation/absorption in a porous medium. Mahdy et al. [19] have discussed the magnetohydrodynamic free convection from a wavy cone to a porous medium at high Darcy–Rayleigh numbers. In the present problem we examine the composite effects of magnetic field, buoyancy, heat generation and also Darcian and Forchheimer drag forces on the boundary layer convection from an isothermal sphere embedded in a porous regime. To the authors' knowledge, such a study requires further analysis which is of interest to the heat transfer community.

2. Mathematical flow model

Let us consider the steady laminar boundary layer heat transfer in an incompressible, viscous, electrically-conducting fluid on a spherical body immersed in a fluid-saturated porous medium. The ambient fluid temperature is T_∞. A constant transverse magnetic field with strength, B_o, is applied along the coordinate, Y, as indicated in Fig. 1. The surface temperature of the sphere is maintained at T_w, a value in excess of T_∞. It is assumed that the magnetic Reynolds number $R_m = \mu_o a W L \ll 1$, where μ_o is the magnetic permeability, a is the radius of the sphere, L and W are the characteristic length and velocity, respectively. Under these conditions it is possible to neglect the effect of the induced magnetic field as compared with the applied magnetic field. Viscous and Joule heating effects are also neglected. The X-coordinate is directed along the sphere surface from the stagnation point and the Y-coordinate defines distance normal to the sphere surface. The fluid possesses constant thermophysical properties with the exception of those caused by density changes which generate the buoyancy force, under the Boussinesq approximation. It is also assumed that the effect of the buoyancy-induced streamwise pressure gradient terms on the flow and temperature fields is negligible. Under these assumptions, the boundary layer equations, based on the conservation of mass, momentum and energy can be shown to reduce to:

$$\frac{\partial (RU)}{\partial X} + \frac{\partial (RV)}{\partial Y} = 0 \tag{1}$$

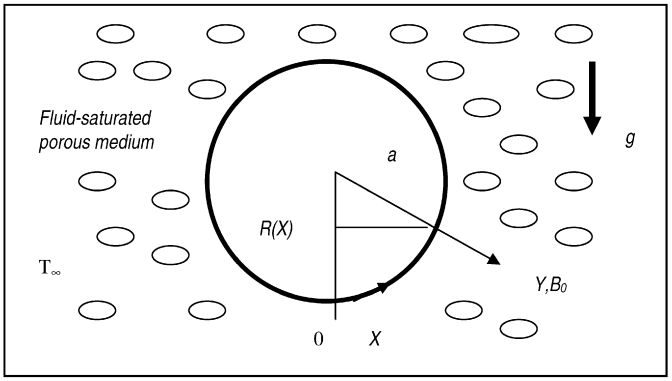

Fig. 1. Geometry of physical regime.

$$\rho\left(U\frac{\partial U}{\partial X}+V\frac{\partial U}{\partial Y}\right)=\mu\left(\frac{\partial^2 U}{\partial Y^2}\right)+\rho g\beta(T-T_\infty)\sin\left(\frac{X}{a}\right)-\sigma B_o^2 U-\frac{\mu}{K}U-\frac{\rho b U^2}{K} \tag{2}$$

$$\rho\left(U\frac{\partial T}{\partial X}+V\frac{\partial T}{\partial Y}\right)=\frac{k}{\rho c_p}\left(\frac{\partial^2 T}{\partial Y^2}\right)+\frac{Q_o}{\rho c_p}[T-T_\infty] \tag{3}$$

The corresponding wall and free stream boundary conditions are, respectively:

$$\text{At } Y=0: \qquad U=0, \quad V=0, \quad T=T_w \tag{4a}$$

$$\text{As } Y\to\infty: \quad U\to 0, \quad T\to T_\infty \tag{4b}$$

where U, V are the velocity components in the X, Y directions respectively, σ is the electrical conductivity of the fluid, T is the temperature, ρ is the fluid density, μ is the dynamic viscosity, g denotes gravitational acceleration, $R(X)=a\sin(X/a)$ denotes the radial distance from the symmetrical axis to the sphere surface, K is the permeability of the porous medium, b is the Forchheimer drag coefficient, β is the coefficient of thermal expansion, c_p is the specific heat at constant volume, $Q_o(T-T_\infty)$ is the quantity of heat generation/absorption per unit volume, Q_o is a constant. The subscripts w and ∞ denote conditions on the surface of the sphere and in the free stream, respectively. Proceeding with the analysis we now introduce the following variables, following Molla et al. [6]:

$$x=\left(\frac{X}{a}\right), \qquad y=\frac{Y}{a}Gr^{1/4}, \qquad u=\frac{a}{\nu\, Gr^{1/2}}U$$

$$v=\frac{a}{\nu\, Gr^{1/4}}V, \qquad \theta=\frac{T-T_\infty}{T_w-T_\infty}$$

$$Gr=\frac{g\beta(T_w-T_\infty)a^3}{\nu^2}, \qquad Da=\frac{K}{a^2}$$

$$Fs=\frac{b}{a}, \qquad r(x)=a\sin x \tag{5}$$

where x, y are dimensionless coordinates along and normal to the tangent of the sphere surface, u, v are the dimensionless velocities in the x, y directions, Gr is the Grashof number, θ is dimensionless temperature, Da is the Darcy number, Fs is the Forchheimer number, ν is kinematic viscosity. We note that since the porous medium is homogenous and isotropic, only a single permeability, K, is required to simulate it. Also the heat source/sink term, Q_o is greater than zero for heat generation and less than zero for heat absorption. Implementation of the variables (5) in the boundary-layer equations (1) to (3) leads to the following dimensionless partial differential equations:

Mass conservation:

$$\frac{\partial(ru)}{\partial x}+\frac{\partial(rv)}{\partial y}=0 \tag{6}$$

Momentum conservation:

$$\left(u\frac{\partial u}{\partial x}+v\frac{\partial u}{\partial y}\right)=\left(\frac{\partial^2 u}{\partial y^2}\right)+\theta\sin(x)-\frac{\sigma B_o^2 a^2}{\rho\nu Gr^{1/2}}u-\frac{Gr^{1/2}}{Da}u-\frac{Fs\,Gr}{Da}u^2 \tag{7}$$

Energy (heat) conservation:

$$\left(u\frac{\partial\theta}{\partial x}+v\frac{\partial\theta}{\partial y}\right)=\frac{1}{Pr}\left(\frac{\partial^2\theta}{\partial y^2}\right)+\frac{Q_o}{\rho c_p}-\frac{a^2}{\nu\, Gr^{1/2}}\theta \tag{8}$$

where Pr is the Prandtl number. The corresponding dimensionless boundary conditions now take the form:

$$\text{At } y=0: \qquad u=v=0; \quad \theta=1 \tag{9a}$$

$$\text{As } y\to\infty: \quad u\to 0, \quad \theta\to 0 \tag{9b}$$

We further define a stream function as follows:

$$\psi(x,y)=xr(x)f(x,y) \tag{10}$$

and define using the Cauchy–Riemann equations:

$$u=\frac{1}{r}\frac{\partial\psi}{\partial y} \tag{11a}$$

$$v=-\frac{1}{r}\frac{\partial\psi}{\partial x} \tag{11b}$$

The dimensionless equations (6) to (8) now become:

$$\left(\frac{\partial^3 f}{\partial y^3}\right)+\left(1+\frac{x}{\tan x}\right)f\frac{\partial^2 f}{\partial y^2}-\left[\frac{\partial f}{\partial y}\right]^2+\frac{\theta}{x}\sin(x)-Nm\frac{\partial f}{\partial y}-\frac{Gr^{1/2}}{Da}\left[\frac{\partial f}{\partial y}\right]-\frac{Fs\,Gr}{Da}x\left[\frac{\partial f}{\partial y}\right]^2=x\left[\frac{\partial f}{\partial y}\frac{\partial^2 f}{\partial y\partial x}-\frac{\partial f}{\partial x}\frac{\partial^2 f}{\partial y^2}\right] \tag{12}$$

$$\frac{1}{Pr}\left(\frac{\partial^2\theta}{\partial y^2}\right)+\left(1+\frac{x}{\tan x}\right)f\frac{\partial\theta}{\partial y}+H\theta=x\left[\frac{\partial f}{\partial y}\frac{\partial\theta}{\partial x}-\frac{\partial f}{\partial x}\frac{\partial\theta}{\partial y}\right] \tag{13}$$

where $Nm=\frac{\sigma B_o^2 a^2}{\mu\, Gr^{1/2}}$ is the hydromagnetic parameter and $H=\frac{a^2 Q_o}{c_p\mu\, Gr^{1/2}}$ is the heat source/sink parameter. The transformed boundary conditions finally take the form:

$$\text{At } y=0: \qquad f=\frac{\partial f}{\partial y}=0; \quad \theta=1 \tag{14a}$$

$$\text{As } y\to\infty: \quad \frac{\partial f}{\partial y}\to 0, \quad \theta\to 0 \tag{14b}$$

The two-point boundary value problem defined by Eqs. (12), (13) subject to the surface and free stream conditions (14a) and (14b) is well-posed and can be solved by a variety of numerical methods. Analytical solutions are intractable however. We elect to use the Network Simulation Method (NSM) which is discussed in due course. The flow regime is controlled by six thermophysical parameters, namely *Nm*, *Da*, *Gr*, *Fs*, *Pr* and *H*. In order to provide comparisons with simplifications of the present model we shall discuss now certain special cases of the general flow model.

Case I. Lower stagnation point MHD Heat transfer with heat generation or absorption in a Darcian porous medium. Following Molla et al. [6], we observe that for $x \sim 0$, in the vicinity of the *lower stagnation point* on the sphere, the momentum and energy equations can be simplified to the following coupled ordinary differential equations:

$$\left(\frac{d^3 f}{dy^3}\right) + 2f\frac{d^2 f}{dy^2} - \left[\frac{df}{dy}\right]^2 + \theta - Nm\frac{\partial f}{\partial y} - \frac{Gr^{1/2}}{Da}\left[\frac{\partial f}{\partial y}\right] = 0 \tag{15}$$

$$\frac{1}{Pr}\left(\frac{d^2\theta}{dy^2}\right) + 2f\frac{d\theta}{dy} + H\theta = 0 \tag{16}$$

Case II. Heat transfer without magnetic field or heat generation/absorption effects in a purely fluid medium. With $Nm = 0$ (electrically non-conducting), $H = 0$ (no heat source or sink), $Da \to \infty$ (i.e. when porous fibers vanish in the limit), Eqs. (12) and (13) become:

$$\left(\frac{\partial^3 f}{\partial y^3}\right) + \left(1 + \frac{x}{\tan x}\right) f\frac{\partial^2 f}{\partial y^2} - \left[\frac{\partial f}{\partial y}\right]^2 + \frac{\theta}{x}\sin(x) = x\left[\frac{\partial f}{\partial y}\frac{\partial^2 f}{\partial y \partial x} - \frac{\partial f}{\partial x}\frac{\partial^2 f}{\partial y^2}\right] \tag{17}$$

$$\frac{1}{Pr}\left(\frac{\partial^2\theta}{\partial y^2}\right) + \left(1 + \frac{x}{\tan x}\right) f\frac{\partial\theta}{\partial y} = x\left[\frac{\partial f}{\partial y}\frac{\partial\theta}{\partial x} - \frac{\partial f}{\partial x}\frac{\partial\theta}{\partial y}\right] \tag{18}$$

This case has been studied by Molla et al. [6] and the same equations can also be extracted from the micropolar convection study by Nazar et al. [20] and the Newtonian study by Huang and Chen [21]. Further of interest in engineering design we define a local Nusselt number as follows:

$$Nu_x = -\frac{\partial\theta(x,0)}{\partial y} \tag{19}$$

This allows an estimate to be made of the rate of heat transfer at the surface of the sphere.

3. Numerical solution by Network Simulation Method (NSM)

The governing equations (12) and (13) under boundary conditions (14a) and (14b) amount to a *fifth* order set of nonlinear, coupled partial differential equations with five corresponding boundary conditions. The NSM has been applied successfully to an extensive range of linear and non-linear transport problems [22–28]. In the NSM technique, discretization of the differential equations is founded on the *finite-difference* formulation, where discretization of the spatial coordinates is necessary. It is assumed that the electrical variable of voltage is equivalent to the velocities (U, V) and temperature (T), while the current is equivalent to the velocity flux $(\partial U/\partial X, \partial U/\partial Y, \partial V/\partial Y)$ and temperature flux $(\partial T/\partial X, \partial T/\partial Y)$. A network electrical model for *each* volume element is designed so that its electrical equations are formally equivalent to the spatial discretized equation. The entire network model, including the devices associated with the boundary conditions, is solved by the numerical computer code Pspice [29]. This code is imposed and adjusted continuously automatically for the time-step to reach a convergent solution in each iteration, according to the given stability and convergence requirements. Eqs. (12) and (13) may be further written as:

For $x \sim 0$:

$$\left(\frac{d^2 h}{dy^2}\right) + 2f\frac{dh}{dy} - h^2 + \theta - Nm\,h - \frac{Gr^{1/2}}{Da}h = 0 \tag{20}$$

$$\frac{1}{Pr}\left(\frac{d^2\theta}{dy^2}\right) + 2f\frac{d\theta}{dy} + H\theta = 0 \tag{21}$$

where

$$\frac{df}{dy} = h \tag{22}$$

For $x > 0$:

$$\left(\frac{\partial^2 h}{\partial y^2}\right) + \left(1 + \frac{x}{\tan x}\right) f\frac{\partial h}{\partial y} - h^2 + \frac{\theta}{x}\sin(x) - Nm\,h - \frac{Gr^{1/2}}{Da}h - \frac{Fs\,Gr}{Da}xh^2 = x\left[h\frac{\partial h}{\partial x} - \frac{\partial f}{\partial x}\frac{\partial h}{\partial y}\right] \tag{23}$$

$$\frac{1}{Pr}\left(\frac{\partial^2\theta}{\partial y^2}\right) + \left(1 + \frac{x}{\tan x}\right) f\frac{\partial\theta}{\partial y} + H\theta = x\left[h\frac{\partial\theta}{\partial x} - \frac{\partial f}{\partial x}\frac{\partial\theta}{\partial y}\right] \tag{24}$$

The NSM technique begins with the design of the network model of the element cell, following which we incorporate the boundary conditions. The following currents are defined:

$$J_{h,y} = \frac{\partial h}{\partial y} \tag{25a}$$

$$J_{h,x} = \frac{\partial h}{\partial x} \tag{25b}$$

$$J_{\theta,y} = \frac{\partial\theta}{\partial y} \tag{25c}$$

$$J_{\theta,x} = \frac{\partial\theta}{\partial x} \tag{25d}$$

$$J_{f,x} = \frac{\partial f}{\partial x} \tag{25e}$$

With these definitions of the currents, Eqs. (23) and (24) can be cast as follows:

Table 1
Nu_x computations for non-magnetic convection from a sphere without heat generation for $Pr = 0.7, 7.0$

x (degrees)	$Pr = 0.7$				$Pr = 7.0$			
	Ref. [6]	Ref. [20]	Ref. [21]	NSM	Ref. [6]	Ref. [20]	Ref. [21]	NSM
0	0.4576	0.4576	0.4574	0.4577	0.9582	0.9595	0.9581	0.9591
10	0.4564	0.4565	0.4563	0.4564	0.9558	0.9572	0.9559	0.9569
20	0.4532	0.4533	0.4532	0.4534	0.9492	0.9506	0.9496	0.9499
30	0.4479	0.4480	0.4480	0.4481	0.9383	0.9397	0.9389	0.9392
40	0.4404	0.4405	0.4407	0.4409	0.9231	0.9239	0.9239	0.9243
50	0.4307	0.4308	0.4312	0.4313	0.9034	0.9045	0.9045	0.9047
60	0.4188	0.4189	0.4194	0.4192	0.8791	0.8801	0.8805	0.8803
70	0.4045	0.4046	0.4053	0.4051	0.8501	0.8510	0.8518	0.8515
80	0.3877	0.3879	0.3886	0.3885	0.8161	0.8168	0.8182	0.8178
90	0.3863	0.3684	0.3694	0.3692	0.7768	0.7774	0.7792	0.7785

$$\frac{\partial J_{h,y}}{\partial y} + \left(1 + \frac{x}{\tan x}\right) f J_{h,y} - h^2 + \frac{\theta}{x}\sin(x) - Nm\,h - \frac{Gr^{1/2}}{Da}h - \frac{Fs\,Gr}{Da}xh^2 = x[h J_{h,x} - J_{f,x} J_{h,y}] \tag{26}$$

$$\frac{\partial J_{\theta,y}}{\partial y} + Pr\left(1 + \frac{x}{\tan x}\right) f J_{\theta,y} + Pr\,H\theta = xPr[h J_{\theta,x} - J_{f,x} J_{\theta,y}] \tag{27}$$

These partial differential equations can be transformed into a system of *connected differential equations*, by means of the spatial discretization, where the following currents (28a)–(28d) are implemented by means of resistors of value "ΔY" and others currents are implemented with the voltage control current generator.

$$J_{h,i,j-\Delta Y} = (h_{i,j-\Delta Y} - h_{i,j})/\Delta Y \tag{28a}$$

$$J_{h,i,j+\Delta Y} = (h_{i,j} - h_{i,j+\Delta Y})/\Delta Y \tag{28b}$$

$$J_{\theta,i,j-\Delta Y} = (\theta_{i,j-\Delta Y} - \theta_{i,j})/\Delta Y \tag{28c}$$

$$J_{\theta,i,j+\Delta Y} = (\theta_{i,j} - \theta_{i,j+\Delta Y})/\Delta Y \tag{28d}$$

A *first-order* central difference approximation is used for the first derivate (Eqs. (25a) and (25c)), a first-order non-central difference approximation is used in Eqs. (25b), (25d), and (25e) and finally a *second-order* central difference approximation is used for the second derivate (Eqs. (28a)–(28d)).

$$J_{h,y} = \frac{\partial h}{\partial y} \approx \frac{h_{i,j+\Delta y} - h_{i,j-\Delta y}}{2\Delta y} \tag{29a}$$

$$J_{\theta,y} = \frac{\partial \theta}{\partial y} \approx \frac{\theta_{i,j+\Delta y} - \theta_{i,j-\Delta y}}{2\Delta y} \tag{29b}$$

$$J_{h,x} = \frac{\partial h}{\partial x} \approx \frac{h_{i,j+\Delta y} - h_{i,j}}{\Delta x} \tag{29c}$$

$$J_{\theta,x} = \frac{\partial \theta}{\partial x} \approx \frac{\theta_{i,j+\Delta y} - \theta_{i,j}}{\Delta x} \tag{29d}$$

$$J_{f,x} = \frac{\partial f}{\partial x} \approx \frac{f_{i,j+\Delta y} - f_{i,j}}{\Delta x} \tag{29e}$$

$$\frac{\partial J_{h,y}}{\partial y} \approx \frac{J_{h,i,j-\Delta y} - J_{h,i,j+\Delta y}}{\Delta y} = \frac{h_{i,j-\Delta y} + h_{i,j+\Delta y} - 2h_{i,j}}{\Delta y^2} \tag{29f}$$

$$\frac{\partial J_{\theta,y}}{\partial y} \approx \frac{J_{\theta,i,j-\Delta y} - J_{\theta,i,j+\Delta y}}{\Delta y} = \frac{\theta_{i,j-\Delta y} + \theta_{i,j+\Delta y} - 2\theta_{i,j}}{\Delta y^2} \tag{29g}$$

In Eqs. (26) and (27) all the terms can be treated as a current. Therefore implementing Kirchhoff's law for electrical currents from circuit theory, the network model is obtained. To introduce the boundary conditions, voltage sources are employed to simulate constant values of velocity and temperature. Similarly, Eqs. (20) and (21) can be modeled by means of the NSM and it is possible to obtain the numerical solutions to $x = 0$. These are subsequently input as boundary conditions for a solution for $x > 0$, which is two-dimensional.

4. Results and discussion

To test the validity of the present numerical solutions we have compared the NSM computations with selected results in Molla [6], Nazar et al. [20] and Huang and Chen [21]. Table 1 provides the solutions for Nu_x, i.e. local Nusselt number $(= -\partial\theta(x,0)/\partial y)$ obtained in [6,20] and [21] along with the present NSM results, for the cases of air, i.e. $Pr = 0.7$ and water for which $Pr = 7.0$. In the case of Ref. [20] the micropolar flow equations can be shown to reduce to (17) and (18) for the Newtonian case. In the case of Ref. [21] when transpiration (i.e. suction or blowing) effects are neglected, the resulting equations are identical to (17) and (18) and the data in Table 1 is for the prescribed surface temperature case considered by Huang and Chen [21]. Table 2 provides solutions for the dimensionless shear stress function $\partial^2 f(x,0)/\partial y^2$ obtained by Huang and Chen [21] for the prescribed surface temperature case, for $Pr = 0.7$ (air) and $Pr = 7.0$. These computations were obtained with the Keller-box finite difference method. In the NSM computations shown in Figs. 2 to 12, default values for the governing dimensionless numbers are as follows: $Nm = 1$, $Da = 0.1$, $Gr = 1$, $Fs = 1$, $Pr = 0.7$ and $H = 0$, unless otherwise indicated. As such the figures correspond to *hydromagnetic thermal convection in electrically conducting air-saturated non-Darcian porous media, without heat sources*. Excellent agreement of the present NSM computations, with the earlier solutions of Molla et al. [6] in the absence of porous body forces ($Da \to \infty$ and $Fs = 0$), with Nazar et al. [20]

Table 2
Dimensionless shear stress ($\frac{\partial^2 f(x,0)}{\partial y^2}$) computations for electrically non-conducting convection from a sphere without heat generation for $Pr = 0.7, 7.0$

x (degrees)	Ref. [21] $Pr = 0.7$	NSM $Pr = 0.7$	Ref. [21] $Pr = 7.0$	NSM $Pr = 7.0$
0	0.7678	0.7680	0.5034	0.5026
10	0.7655	0.7658	0.5019	0.5023
20	0.7586	0.7590	0.4975	0.4982
30	0.7471	0.7473	0.4901	0.4900
40	0.7311	0.7310	0.4800	0.4811
50	0.7108	0.7111	0.4670	0.4682
60	0.6863	0.6868	0.4514	0.4518
70	0.6577	0.6583	0.4332	0.4336
80	0.6253	0.6261	0.4127	0.4134
90	0.5892	0.5898	0.3898	0.3907

neglecting micropolar effects and with Huang and Chen [21] neglecting transpiration effects, is achieved in Table 1, up to three decimal places. In Table 2, the NSM computations are again found to show excellent agreement with selected solutions by Huang and Chen [21], for the dimensionless shear stress for electrically *non-conducting purely fluid convection from a sphere without heat generation* ($Da \to \infty$, $Fs = 0$, $Nm = 0$, $H = 0$) for $Pr = 0.7$ (air), 7.0 (water). In Table 1 we observe that local Nusselt number, Nu_x, decreases steadily with an increase in x. Therefore as we progress from the lower stagnation point on the sphere ($x \sim 0$) through increments of 10 degrees, up to $x = 90$ degrees, for the case of air ($Pr = 0.7$) Nu_x falls from 0.7680 to 0.5898. Similarly a decrease in Nu_x also occurs for the case of water ($Pr = 7.0$), i.e. the Nu_x values decreases from 0.5026 for $x = 0$ degrees to 0.3907 for $x = 90$ degrees. With an increase in Prandtl number there is therefore marked reduction in Nu_x values, i.e. heat transfer rates at the sphere surface are decreased. In Table 2 shear stress function, $\partial^2 f(x,0)/\partial y^2$, is also observed to decrease continuously, for both $Pr = 0.7$ and $Pr = 7.0$, as x increases, i.e. as we progress from the lower stagnation point around the sphere to the outermost point on the sphere surface (at $x = 90$ degrees). However values corresponding to $Pr = 0.7$ are significantly larger than for $Pr = 7.0$. Shear stress function for $Pr = 0.7$ falls from 0.7680 at $x = 0$, to 0.5898 for $x = 90$ degrees ($\pi/2$ radians) and for $Pr = 7.0$, shear stress function decreases from 0.5026 at $x = 0$ degrees to 0.3907 at $x = 90$ degrees ($\pi/2$ radians). Clearly therefore for either $Pr = 0.7$ and $Pr = 7.0$, the maximum surface heat transfer and surface shear stress function occurs always at the lower stagnation point on the sphere.

In Figs. 2 and 3 the influence of Darcy number, Da on the velocity, $[\partial f/\partial y]$, and temperature function, θ, profiles versus transverse coordinate (normal to the sphere surface) is shown, both for the case of *non-Darcian MHD convection with heat generation*. As Da is increased from 0.01 (low permeability) through 0.05, 0.1 and 1.0 (very high permeability) a marked increase in velocity occurs. The Darcian impedance term in $-Gr^{1/2}/Da[\partial f/\partial y]$ in the momentum equation (12) is clearly inversely proportional to Da, for constant Gr. With less fibers to resist the flow, i.e. with greater permeability (corresponding to an increase in Darcy number) there will be a reduction in the Darcian drag acting on the flow regime which will serve to

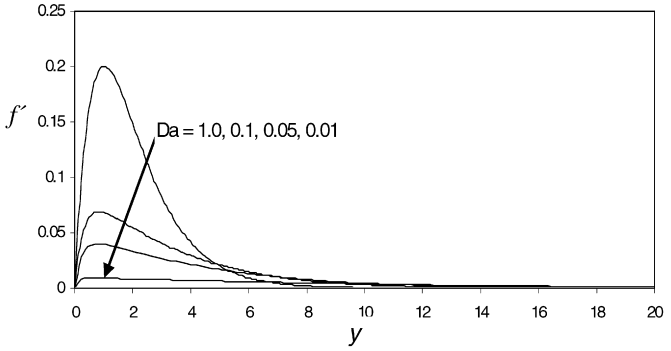

Fig. 2. Velocity variation for various Darcy numbers (Da).

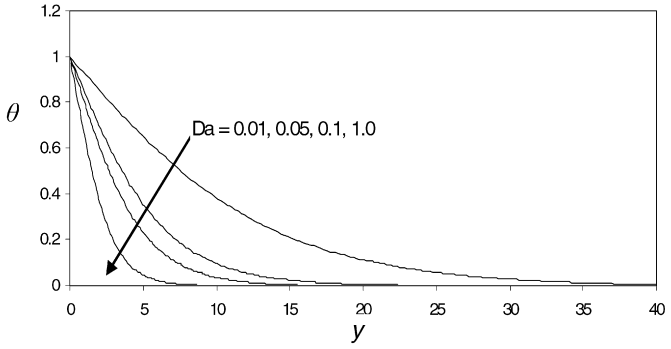

Fig. 3. Temperature variation for various Darcy numbers (Da).

progressively accelerate the flow, consistent with the trend for increasing velocity in Fig. 2. The implication of this in practical systems is that more permeable materials which contain less solid fibers will provide a *decreased inhibition* to flow. Maximum velocities are located near to the sphere surface in the boundary-layer regime, and these decay to zero in the free stream. Conversely with an increase in Da, the temperature in the flow domain, θ, is seen to *decrease* substantially. With larger permeabilities less solid material is present in the regime for thermal conduction heat transfer and this acts to decrease temperatures in the saturated regime. Maximum temperature is always located at the sphere surface ($y = 0$) and decays smoothly to zero as we approach the free stream. As such the presence of a porous medium serves as a strong control mechanism in industrial operations where the flow can be regulated and also temperatures reduced.

In Figs. 4 and 5 the effects of hydromagnetic parameter, Nm, on the velocity and temperature distributions through the boundary layer are illustrated. The case of $Nm = 0$ implies *electrically non-conducting flow*. For $Nm = 1$ the hydromagnetic drag force (Lorentz body force) is of the same order of magnitude as the viscous hydrodynamic force in the boundary layer. An increase in Nm corresponds therefore to an increase in the magnitude of magnetic field applied in the y direction (normal to the sphere surface) and serves to decrease velocity in the regime, owing to the increase in hydromagnetic drag. In consistency with the classical investigations of Gardner et al. [30] and Bush [31], a *velocity overshoot* is observed. Velocity is therefore seen to peak in the vicinity of the sphere surface and then decrease rapidly to zero in the free stream.

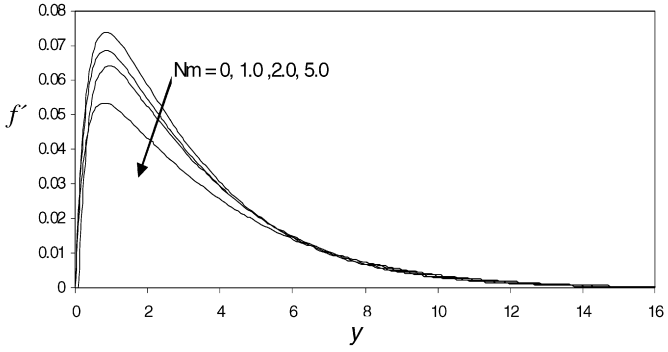

Fig. 4. Velocity variation for various hydromagnetic parameters (Nm).

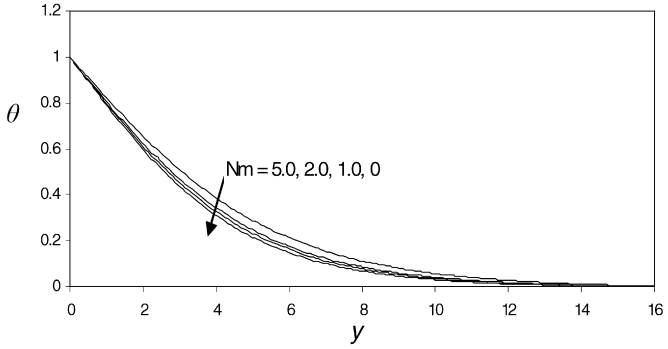

Fig. 5. Temperature variation for various hydromagnetic parameters (Nm).

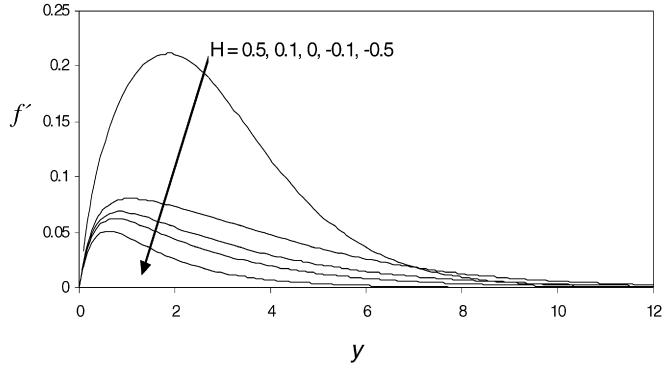

Fig. 6. Velocity variation for various heat source/sink parameters (H).

The maximum velocity clearly corresponds to the electrically non-conducting case ($Nm = 0$). Conversely we observe that an increase in Nm causes a marked rise in the temperature, θ, in the fluid. With increasing magnetic field, more energy is dissipated in the fluid and this manifests as an increase in thermal energy which serves to boost temperatures. The greatest difference in θ profiles occurs some distance from the sphere. In consistency with the boundary conditions specified in (14a) and (14b) maximum temperature always arises at the wall and then decreases smoothly to zero in the free stream (far away from the sphere surface).

In Figs. 6 and 7 we have presented the influence of the heat source/sink parameter, H, on the velocity and temperature profiles in the boundary-layer regime. The presence of a heat source ($H > 0$), i.e. heat generation, creates a *hot layer* adjacent to the surface of the sphere which decreases the heat transfer rate from the surface. Conversely with a heat sink present ($H < 0$), i.e. heat absorption, a *cold layer* of fluid is generated adjacent to the sphere surface which serves to increase heat transfer rates from the surface. Velocity, $[\partial f/\partial y]$, is seen to increase substantially with heat source ($H = 0.1, 0.5$) and decrease with heat sink ($H = -0.1, -0.5$). The maximum velocity corresponds to the maximum heat source case, $H = 0.5$, and occurs at $y \sim 2$, i.e. relatively close to the sphere surface. All velocity profiles decay to zero in the free stream. The temperature in the fluid-saturated porous regime, θ, clearly increases with heat generation present as thermal energy is added to the flow regime for $H = 0.1, 0.5$. Conversely temperatures are decreased for $H = -0.1, -0.5$, i.e. with heat absorption present. The case with no heat generation/absorption ($H = 0$) clearly falls between $H = 0.1$ and $H = -0.1$. All temperature profiles decrease to zero gradually as we approach the exterior of the boundary-layer regime.

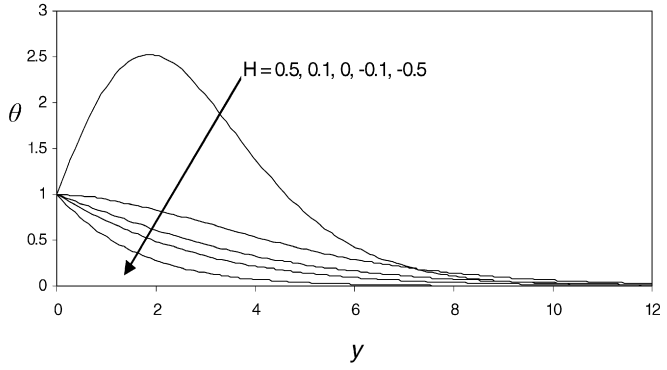

Fig. 7. Temperature variation for various heat source/sink parameters (H).

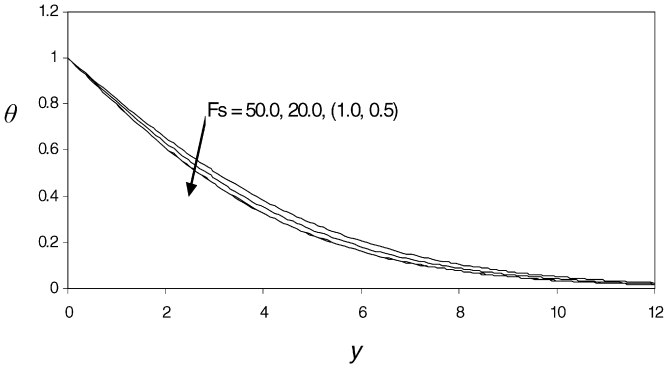

Fig. 8. Temperature variation for various Forchheimer numbers (Fs).

In Fig. 8 the influence of the Forchheimer (second order) porous drag parameter, Fs, on temperature profiles with distance normal to the sphere surface is shown. The Forchheimer drag is an inertial term which appears as $-Fs\,Gr/Dax[\partial f/\partial y]^2$ in the momentum conservation equation (12). As such increasing Fs will increase the Forchheimer drag in the porous medium which will serve to decelerate the flow, i.e. reduce velocities (not shown), and will increase the temperature throughout the boundary layer adjacent to the sphere surface. Peak temperature therefore is associated with the maximum value of Fs, i.e. 50. All profiles decay continuously from a maximum at the sphere surface ($y = 0$) to zero far way from the surface.

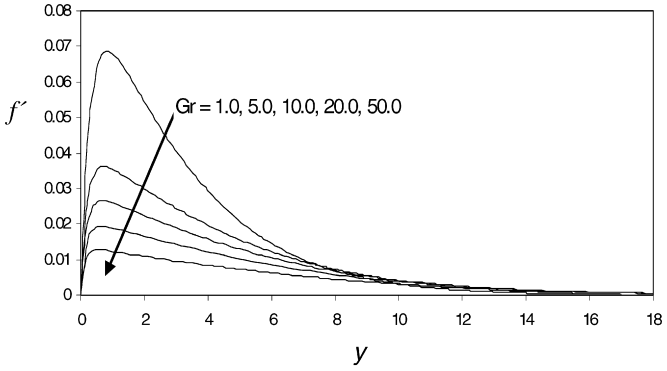

Fig. 9. Velocity variation for various Grashof numbers (Gr).

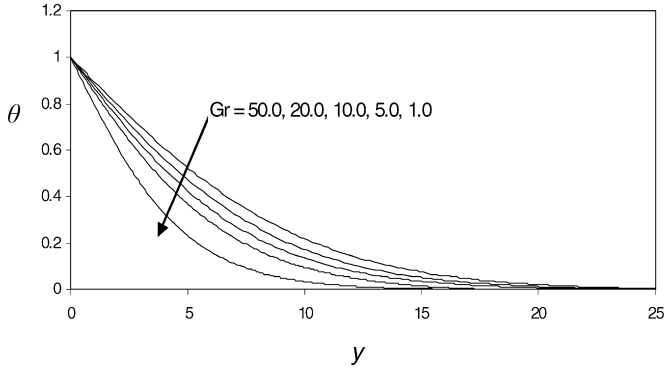

Fig. 10. Temperature variation for various Grashof numbers (Gr).

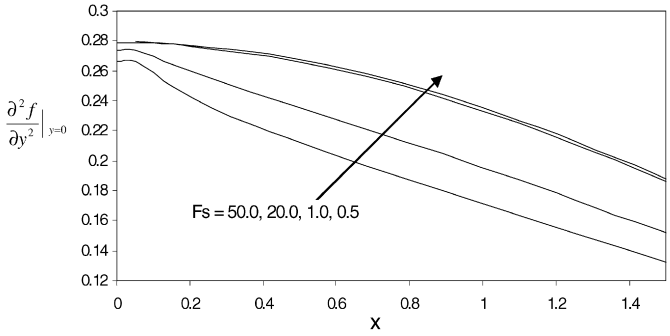

Fig. 11. Surface shear stress function variation for various Forchheimer numbers (Fs).

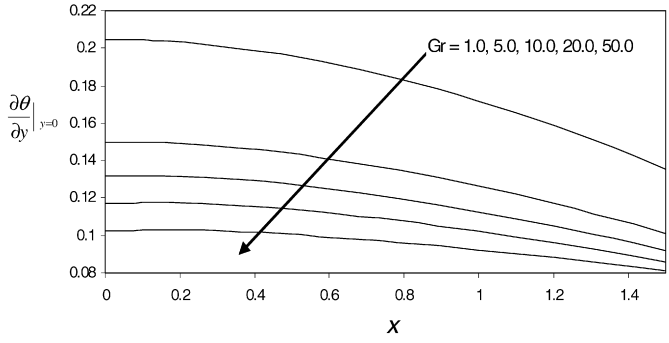

Fig. 12. Surface temperature gradient variation with Grashof number (Gr).

The influence of the free convection parameter, Grashof number (Gr) on velocity and temperature distributions with y coordinate is depicted in Figs. 9 and 10. Increasing Gr corresponds to an increase in thermal buoyancy force in the regime. As such the flow is decelerated which causes the velocity to plummet considerably. Peak velocities (as shown in Fig. 9) correspond to $y \sim 1$ (close to the sphere surface), and fall from 0.068 for $Gr = 1.0$ to 0.012 for $Gr = 50$. There is a sharp rise in velocity near the sphere surface after which velocities peak and then decrease continuously to zero far from the surface. Conversely with an increase in free convection parameter, as seen in Fig. 10, since positive Grashof number implies cooling of the sphere surface by convection currents (i.e. thermal energy transfer to the fluid), there is a substantial increase in temperature in the fluid-saturated porous regime. For $Gr < 0$ there is heating of the sphere surface by free convection currents which would induce cooling of the fluid in the regime, as described by Naroua et al. in [32], although this case has not been shown in the figures, for brevity.

The effects of Fs and Gr on the surface shear stress function, $\partial^2 f(x,0)/\partial y^2$ and surface temperature gradient, $-\partial\theta(x,0)/\partial y$, i.e. negative local Nusselt number function, respectively, with coordinate along the surface, x, are shown in Figs. 11 and 12. The porous medium inertia effects constitute a strong resistance to flow. Increasing Fs, boosts the Forchheimer inertial drag which slows down flow in the medium. Therefore shear stress function is seen to be reduced considerably as Fs increases from 0.5 (weak inertial drag), through 1.0, 20, to 50 (very strong inertial drag). All profiles descend from a maximum at the lower stagnation point ($x = 0$) to a minimum at $x = 1.5$. Increasing Gr values imply cooling of the sphere surface by free convection currents which serves to decelerate the flow and the surface temperature gradient, $\partial\theta(x,0)/\partial y$ is clearly decreased. Peak values are reduced at the lower stagnation point ($x = 0$) from 0.205 for $Gr = 1.0$, to approximately 0.1 for $Gr = 50$.

5. Conclusions

A mathematical model has been developed for the isothermal hydromagnetic convection from a sphere embedded in a fluid-saturated non-Darcian porous medium in the presence of heat generation or absorption. The transformed partial differential equations for momentum and energy conservation have been solved using the Network Simulation Methodology (NSM) technique. Our computations have shown that an increase in magnetic field parameter (Nm) decreases velocity ($\partial f/\partial y$) and increases temperature (θ). An increase in Darcy number (Da) serves to increase velocity and decrease temperature. An increase in Forchheimer number (Fs) reduces velocity in the porous regime, increases temperature and reduces surface shear stress. With increasing heat generation parameter ($H > 0$) velocity in the porous regime is boosted as is temperature. The reverse effects are achieved with a heat sink (i.e. absorption). Increasing Grashof number (Gr) induces a decrease in velocity and surface temperature gradient (local Nusselt number) but increases considerably the temperature in the porous regime. The present model is aimed at elucidating further the heat transfer aspects of the hydromagnetic convection

from a sphere in fluid-saturated non-Darcian porous media and it is hoped that it will serve as a stimulus for future numerical and also experimental studies of immediate interest in geophysical magneto-convection, materials processing and MHD energy systems applications.

Acknowledgements

The authors are extremely grateful to both reviewers for their excellent comments which have substantially improved this paper.

References

[1] L.P. Ohare, Manoeuvering a re-entry body via magneto-gasdynamic forces, Ph.D. Thesis Maryland Univ., College Park, Maryland Univ., College Park, April, 1992.
[2] V.J. Rossow, On flow of electrically conducting fluids over a flat plate in the presence of a transverse magnetic field, Tech. Rep. TN 3971, NACA, South Carolina, USA, 1957.
[3] R.M. Singer, A study of unsteady convective magnetohydrodynamic channel flow, Argonne National Laboratory report, ANL-6937, November, 1964.
[4] P.C. Kieffer, Variable conductivity fully developed MHD channel flow, Aerospace Research Laboratories Report, ARL 67-46, USAF, February, 1967.
[5] O.A. Bég, H.S. Takhar, G. Nath, A.J. Chamkha, Mathematical modelling of hydromagnetic convection from a rotating sphere with impulsive motion and buoyancy effects, Nonlinear Analysis: Modelling and Control 12 (1) (2007) 227–245.
[6] M.A. Molla, M.A. Taher, M.M.K. Chowdhury, M.A. Hossain, Magnetohydrodynamic natural convection flow on a sphere in presence of heat generation, Nonlinear Analysis: Modelling and Control 10 (4) (2007) 349–363.
[7] M. Kumari, H.S. Takhar, G. Nath, Compressible MHD boundary layer in the stagnation region of a sphere, Int. J. Engineering Science 28 (1990) 357–366.
[8] M. Molla, M. Hossain, M. Taher, Magnetohydrodynamic natural convection flow on a sphere with uniform heat flux in presence of heat generation, Acta Mechanica 186 (1–4) (2006) 75–86.
[9] M. Alam, M.A. Alim, M.K. Chowdhury, Viscous dissipation effects on MHD natural convection flow along a sphere, J. Mechanical Engineering 36 (2006) 44–50.
[10] A.J. Chamkha, A. Al-Mudhaf, Simultaneous heat and mass transfer from a permeable sphere at uniform heat and mass fluxes with magnetic field and radiation effects, Numerical Heat Transfer: Part A—Applications 46 (2) (2004) 181–198.
[11] H.S. Takhar, G. Nath, Self-similar solution of the unsteady flow in the stagnation point region of a rotating sphere with a magnetic field, Heat and Mass Transfer 36 (2) (2000) 89–96.
[12] H.S. Takhar, A.J. Chamkha, G. Nath, Unsteady laminar MHD flow and heat transfer in the stagnation region of an impulsively spinning and translating sphere in the presence of buoyancy forces, Heat and Mass Transfer 37 (4) (2001) 397–402.
[13] K.A. Yih, Viscous and Joule heating effects on non-Darcy MHD natural convection flow over a permeable sphere in porous media with internal heat generation, Int. Comm. Heat Mass Transfer 27 (4) (2000) 591–600.
[14] R.A. Damseh, Magnetohydrodynamics-mixed convection from radiate vertical isothermal surface embedded in a saturated porous media, ASME J. Applied Mechanics 73 (1) (2006) 54–59.
[15] M. Al-Zubi, H.M. Duwairi, MHD convection over non isothermal ellipse embedded in fluid saturated porous medium, Int. J. Heat Technology 25 (2) (2007) 29–35.
[16] A. Afify, Effects of temperature-dependent viscosity with Soret and Dufour numbers on non-Darcy MHD free convective heat and mass transfer past a vertical surface embedded in a porous medium, Transport in Porous Media 66 (3) (2007) 391–401.
[17] A.M. Rashad, Influence of radiation on MHD free convection from a vertical flat plate embedded in porous media with thermophoretic deposition of particles, Comm. Nonlinear Science Numerical Simulation 13 (10) (2008) 2213–2222.
[18] S.M.M. EL-Kabeir, M.A. EL-Hakiem, A.M. Rashad, Lie group analysis of unsteady MHD three dimensional natural convection from an inclined stretching surface in a saturated porous medium, J. Computational Applied Mathematics 213 (2) (2008) 582–603.
[19] A. Mahdy, R.A. Mohamed, F.M. Hady, Influence of magnetic field on natural convection flow near a wavy cone in porous media, Latin American Applied Research 38 (2008) 155–160.
[20] R. Nazar, N. Amin, T. Grosan, I. Pop, Free convection boundary layer on an isothermal sphere in a micropolar fluid, Int. Comm. Heat Mass Transfer 29 (3) (2002) 377–386.
[21] M.J. Huang, C.K. Chen, Laminar free convection from a sphere with blowing and suction, ASME J. Heat Transfer 109 (1987) 529–532.
[22] J. Zueco, F. Alhama, Inverse estimation of temperature dependent emissivity of solid metals, J. Quantitative Spectroscopy Radiative Transfer 101 (2006) 73–86.
[23] J. Zueco, F. Alhama, Simultaneous inverse determination of the temperature-dependent thermophysical properties of fluids using the network simulation method, Int. J. Heat Mass Transfer 50 (2007) 3234–3243.
[24] F. Alhama, J. Zueco, Application of the lumped model to solids with linearly temperature-dependent thermal conductivity, Applied Mathematical Modelling 31 (2007) 302–310.
[25] J. Zueco, Numerical study of an unsteady free convective magnetohydrodynamic flow of a dissipative fluid along a vertical plate subject to constant heat flux, Int. J. Engineering Science 44 (2006) 1380–1393.
[26] J. Zueco, Network simulation method applied to radiation and viscous dissipation effects on MHD unsteady free convection over vertical porous plate, Applied Mathematical Modelling 31 (9) (2007) 2019–2033.
[27] J. Zueco, O.A. Bég, H.S. Takhar, A. Sajid, R. Bhargava, Transient Couette flow in a rotating non-Darcian porous medium parallel plate configuration: Network simulation method solutions, Acta Mechanica (2008), in press.
[28] O.A. Bég, J. Zueco, H.S. Takhar, Unsteady magnetohydrodynamic Hartmann–Couette flow and heat transfer in a Darcian channel with Hall current, ionslip, viscous and Joule heating effects: network numerical solutions, Communications in Nonlinear Science and Numerical Simulation (2008), in press.
[29] Pspice 6.0. Irvine, California 92718. Microsim Corporation, 20 Fairbanks (1994).
[30] R.A. Gardner, K.L. Uherka, P.S. Lykoudis, Influence of a transverse magnetic field on forced convection liquid metal heat transfer, AIAA Journal 4 (1966) 848–852.
[31] W.B. Bush, The stagnation point boundary layer in the presence of an applied magnetic field, J. Aerospace Sciences 28 (8) (1961) 610–611.
[32] N. Naroua, H.S. Takhar, P.C. Ram, T.A. Bég, O.A. Bég, R. Bhargava, Transient rotating hydromagnetic partially-ionized heat-generating gas dynamic flow with Hall/ion-slip current effects: finite element analysis, Int. J. Fluid Mechanics Research 34 (6) (2007) 493–505.